EEG Extended Source Imaging with Variation Sparsity and L_p-Norm Constraint

Shu Peng[1], Feifei Qi[3], Hong Yu[1,2], and Ke Liu[1,2](✉)

[1] School of Computer Science and Technology, Chongqing University of Posts and Telecommunications, Chongqing 400065, China
`liuke@cqupt.edu.cn`
[2] Key Laboratory of Big Data Intelligent Computing, Chongqing University of Posts and Telecommunications, Chongqing, China
[3] School of Internet Finance and Information Engineering, Guangdong University of Finance, Guangzhou 510521, China

Abstract. Accurately reconstructing the location and extent of cortical sources is crucial for cognitive research and clinical applications. Regularization methods that use the L_1-norm in the spatial variation domain effectively estimate cortical extended sources. However, in the variation domain, employing L_1-norm constraint tends to overestimate the extent of sources. Hence, to achieve more precise estimations of both the location and extent of sources, further sparseness-enforced regularizations are required. In this work, we develop a robust EEG source imaging method, VSSI-L_p, to estimate extended cortical sources. VSSI-L_p employs the L_p-norm ($0 < p < 1$) in the variation domain to promote sparsity. Using alternating direction method of multipliers (ADMM) and generalized soft-thresholding (GST) algorithm, we can efficiently derive the solution of VSSI-L_p. According to numerical simulations plus real data analysis, VSSI-L_p outperforms both traditional L_2 and L_1-norm-based methods, and the L_1-norm-based method in the variation domain for reconstructing extended sources, validating the outstanding performance of L_p-norm and variation constraint.

Keywords: EEG source imaging · L_p-norm · Variation sparsity · generalized soft-thresholding

1 Introduction

As a non-invasive tool, Electroencephalography (EEG) is used extensively in neuroscience research because of its excellent millisecond-level time resolution. EEG source imaging (ESI) aims to reconstruct cortical activities from EEG signals, essential in neuroscience research and clinical diagnosis (e.g., epileptic seizure area localization). Moreover, ESI can also provide higher spatial resolution in BCIs [6,8], obtaining more precise outcomes.

L. Fang et al. (Eds.): CICAI 2023, LNAI 14474, pp. 500–511, 2024.
https://doi.org/10.1007/978-981-99-9119-8_45

To handle this ESI task, the current density model uses triangles to represent sources and divides the cortex into a fixed triangular mesh [12]. With Maxwell's equations, the EEG signal is somehow a linear combination of the source amplitudes [9]. Then ESI estimates the potential source activities by solving this linear inverse problem, which is to find a source configuration that best suits the scalp EEG measurement. However, the inverse problem is fully underdetermined due to the candidate sources (typically more than 5000) vastly outnumbered the scalp EEG electrodes (tens to hundreds) [7,16]. To obtain a unique source configuration, employing appropriate constraints on the source spaces is therefore necessary.

The most commonly employed constraint is the L_2-norm regularization, like the minimum norm estimate (MNE) [7], which obtains the target source configuration with the minimum energy. However, the solutions of MNE are biased towards superficial sources because the fields generated by scalp sources are stronger than the deep sources with less energy [7]. One way to compensate for this bias is to weight the regularization term with the lead-field matrix, which is referred to as the weighted MNE (wMNE) [13]. Furthermore, in considering the dependencies between adjacent sources, the low-resolution electromagnetic tomography (LORETA) approach was proposed. LORETA minimizes the L_2-norm of the second-order spatial derivative in source space, so as to derive smoothness and local spatial coherent solutions. In general, these L_2-norm-based methods are welcomed due to their computational efficiency, but they limit spatial resolution as they produce diffused estimations, though.

Sparse methods with L_0-norm provide better spatial resolution than the L_2-norm-based approaches, but L_0-norm optimization is computationally infeasible with large-scale data. To approximate the L_0-norm, L_1-norm constraints are commonly used [14]. However, the sparse constraint on the original source space only produces some point sources, providing little information on the size of cortical activities [7,11]. In contrast, employing L_1-norm regularization in the transform domain, such as variation transform, will provide more accurate estimations of extended sources [4,12]. Nonetheless, as suggested in [2], in the transform domain, methods based on L_1-norm tend to overestimate the extent of sources, especially for small-sized sources. Therefore, more sparseness-enforced constraints are necessary to achieve more accurate estimations [3].

To better approximate the solution of L_0-norm with sufficient sparsity, several studies have adopted the L_p-norm ($0 < p < 1$). L_p-norm offers flexible recovery by controlling the value of p. Moreover, L_p-norm-based methods require fewer measurements to achieve reliable reconstruction [3]. Therefore we propose a new ESI algorithm in this work, to accurately estimate locations and extents of sources, named Variation Sparse Source Imaging based on L_p-norm (VSSI-L_p). Specifically, we utilize the L_p-norm regularization for spatial variation sources to obtain sparse and robust solutions in the variation domain. The value of p is alterable to fit sparsity and noise flexibly, enabling more reliable estimations. Moreover, we employ the Alternating Direction Method of Multipliers (ADMM) algorithm [20], in order to solve the optimization problem efficiently.

The structure of this paper is outlined as follows. In Sect. 2, we introduce the details of VSSI-L_p. In Sect. 3, we present the simulation design and evaluation metrics. In Sect. 4, we compare the performance of VSSI-L_p with the benchmark algorithms, followed by a brief discussion and conclusion in Sect. 5.

2 Method

We can use the following formula to describe the linear relationship between potential sources and EEG [2,10]

$$\boldsymbol{b} = \boldsymbol{L}\boldsymbol{s} + \boldsymbol{\varepsilon} \tag{1}$$

in which $\boldsymbol{b} \in \mathbb{R}^{m\times 1}$ is the scalp EEG measurement from m sensors. $\boldsymbol{s} \in \mathbb{R}^{n\times 1}$ denotes the current sources of n sources. $\boldsymbol{L} \in \mathbb{R}^{m\times n}$ is so-called the lead-field matrix, describing the conductivity from potential sources to scalp electrodes. $\boldsymbol{\varepsilon}$ is the measurement noise typically assumed to follow a Gaussian distribution [17].

The goal of ESI is to characterize the location and extents information of potential source $\boldsymbol{s}$ with a giving EEG data $\boldsymbol{b}$. Unfortunately, the number of potential sources n is much bigger than the number of EEG electrodes m, and numerous source configurations are suitable for the scalp measurements. Therefore, narrowing the solution space with constraints is needed for the EEG inverse problem.

$$\boldsymbol{s} = \arg\min_{\boldsymbol{s}} \|\boldsymbol{b} - \boldsymbol{L}\boldsymbol{s}\|_2^2 + f(\boldsymbol{s}) \tag{2}$$

where the former term is the data fitting term, and the latter term is the regularization term which imposes the constraints.

Evidence has revealed that EEG signals largely arise from synchronized neural electrical activity and the cortical activation is compact [1]. Based on this, we assume the sources have the attributes that are locally smooth and globally clustered [10]. To achieve this, we impose sparsity on the variation domain of sources and penalize the differences in amplitude between adjacent dipoles [4]. Specifically, we introduce the variation operator $\boldsymbol{V}$, which is defined as

$$\boldsymbol{V} = \begin{bmatrix} v_{11} & v_{12} & \cdots & v_{1n} \\ v_{21} & v_{22} & \cdots & v_{2n} \\ \vdots & \vdots & \ddots & \vdots \\ v_{P1} & v_{P2} & \cdots & v_{Pn} \end{bmatrix} \begin{cases} v_{pi} = 1, v_{pj} = -1, i < j; & \text{if source i,j share edge p} \\ v_{pi} = 0; & \text{otherwise} \end{cases} \tag{3}$$

Here, P represents the number of edges of all triangular grids in source model. Each row of matrix $\boldsymbol{V}$ refers to the corresponding triangle edge. The values 1 and -1 in the pth row characterize a pair of adjacent sources over the pth edge. Then, each non-zero element in the variation source $\boldsymbol{u} = \boldsymbol{V}\boldsymbol{s} \in \mathbb{R}^{P\times 1}$ denotes the difference of amplitude between the two adjacent sources. To reconstruct locally smooth and globally clustered cortical activities, we assume that the variation source, $\boldsymbol{V}\boldsymbol{s}$, is sparse.

Compared to the L_2-norm and L_1-norm regularization, previous studies have revealed that the L_p-norm $(0 < p < 1)$ can provide more accurate solutions with less measurement data [3]. In this work, we employ the L_p-norm regularization term to develop a precise and robust ESI method, VSSI-*Lp*, to reconstruct extended sources with variation sparsity. The VSSI-*Lp* algorithm intends to solve the following non-convex optimization problem

$$\boldsymbol{s} = \arg\min_{\boldsymbol{s}} \|\boldsymbol{b} - \boldsymbol{L}\boldsymbol{s}\|_2^2 + \lambda\|\boldsymbol{V}\boldsymbol{s}\|_p^p \tag{4}$$

where $\|\cdot\|_p^p = (\sum_i |s_i|^p)$ with $0 < p < 1$, and $\lambda > 0$ is the regularization parameter. In this work, the value of p of the L_p-norm is empirically selected within the result of simulations.

Equation (4) can be rewritten as

$$\boldsymbol{s} = \arg\min_{\boldsymbol{s}} \|\boldsymbol{b} - \boldsymbol{L}\boldsymbol{s}\|_2^2 + \lambda\|\boldsymbol{u}\|_p^p \quad s.t., \boldsymbol{u} = \boldsymbol{V}\boldsymbol{s} \tag{5}$$

which can be efficiently solved using the ADMM algorithm. Hence, the augmented Lagrangian function is derived as

$$\mathcal{L}(\boldsymbol{s}, \boldsymbol{u}, \boldsymbol{z}) = \|\boldsymbol{b} - \boldsymbol{L}\boldsymbol{s}\|_2^2 + \lambda\|\boldsymbol{u}\|_p^p + \boldsymbol{z}^\top(\boldsymbol{V}\boldsymbol{s} - \boldsymbol{u}) + \frac{\rho}{2}\|\boldsymbol{V}\boldsymbol{s} - \boldsymbol{u}\|_2^2 \tag{6}$$

where $\rho > 0$ is the Lagrangian penalty parameter and $\boldsymbol{z} \in \mathbb{R}^{P\times 1}$ is the Lagrangian multiplier. The variables $\boldsymbol{s}, \boldsymbol{u}, \boldsymbol{z}$ can be updated by alternately minimizing the augmented Lagrangian function $\mathcal{L}$. In the kth iteration, these variables are updated as

$$\begin{aligned}
\boldsymbol{s}^{k+1} &= (2\boldsymbol{L}^\top\boldsymbol{L} + \rho\boldsymbol{V}^\top\boldsymbol{V})^{-1}[2\boldsymbol{L}^\top\boldsymbol{b} + \boldsymbol{V}^\top(\rho\boldsymbol{u}^k - \boldsymbol{z}^k)] \\
\boldsymbol{u}^{k+1} &= \arg\min_{\boldsymbol{u}} \lambda\|\boldsymbol{u}\|_p^p + \frac{\rho}{2}\|\boldsymbol{V}\boldsymbol{s}^{k+1} - \boldsymbol{u} + \frac{1}{\rho}\boldsymbol{z}^k\|_2^2 \\
\boldsymbol{z}^{k+1} &= \boldsymbol{z}^k + \rho(\boldsymbol{V}\boldsymbol{s}^{k+1} - \boldsymbol{u}^{k+1})
\end{aligned} \tag{7}$$

Letting $\boldsymbol{y} = \boldsymbol{V}\boldsymbol{s}^{k+1} + \frac{1}{\rho}\boldsymbol{z}^k$, $\boldsymbol{u}^k$ is optimized as

$$\boldsymbol{u}^k = \arg\min_{\boldsymbol{u}} \frac{1}{2}\|\boldsymbol{y} - \boldsymbol{u}\|_2^2 + \frac{\lambda}{\rho}\|\boldsymbol{u}\|_p^p \tag{8}$$

which can be solved using the generalized soft-thresholding (GST) function [21].

In each iteration, we alternately update the variables $\boldsymbol{s}, \boldsymbol{u}, \boldsymbol{z}$. Generally, the iteration is terminated by reaching the maximum number of iterations or when the relative change of the estimated source $\boldsymbol{s}$ reaches the tolerance.

As for application details, the proposed method VSSI-L_p was conducted on a standard PC (Corei9-10980XE CPU 3 GHz and 128 GB RAM). The algorithm will converge after 500 ADMM iterations, which takes about 35 s, for the given simulation configurations in Sect. 3. For reproducibility purposes, the code for the proposed method is available at https://github.com/Mashirops/VSSI-Lp.git.

3 Simulation Design and Performance Metrics

VSSI-Lp is compared with two conventional L_2-norm constraint ESI methods: (1) wMNE [13], (2) LORETA [15], and two sparse constraint methods implemented in the original source domain: (3) L_1-norm regularization [19] which solves

$$\boldsymbol{s}_{L_1} = \arg\min_{\boldsymbol{s}} \|\boldsymbol{b} - \boldsymbol{L}\boldsymbol{s}\|_2^2 + \lambda\|\boldsymbol{s}\|_1, \tag{9}$$

(4) L_p-norm regularization (in this work, we set $p = 0.8$ only for the following formula) [21] which solves

$$\boldsymbol{s}_{L_p} = \arg\min_{\boldsymbol{s}} \|\boldsymbol{b} - \boldsymbol{L}\boldsymbol{s}\|_2^2 + \lambda\|\boldsymbol{s}\|_p^p, \tag{10}$$

and (5) VB-SCCD [4].

3.1 Numerical Simulation

Given the absence of ground truth, several Monte Carlo numerical simulations were conducted with Brainstorm [18], using the default ICBM 152 head structure, to validate the performance of those ESI algorithms. The cortex surface was downsampled into 6004 triangular meshes and each triangular stood for a dipole source perpendicular to the cortical surface. We calculated the lead-field matrix $\boldsymbol{L}$ through BEM models based on the 64-channel Neuroscan Quik-cap sensor system.

On the cortex, we randomly selected a seed triangle and added adjacent triangle grids one by one till the whole area reaches a specified value, so as to construct an extended source. Then we applied an amplitude on the constructed source to obtain the ground truth $\boldsymbol{s}_{real}$. By multiplying it with the lead-field matrix $\boldsymbol{L}$, we obtained the clean EEG signals. To further simulate actual EEG signals for experiments, we added Gaussian white noise on the clean EEG data. By changing the signal-to-noise ratio (SNR), the noise level is controllable. Here, SNR is defined as $10\log_{10}\left[\frac{\sigma^2(\boldsymbol{L}\boldsymbol{s})}{\sigma^2(\varepsilon)}\right]$, where $\sigma^2(\cdot)$ denotes the variance. Monte Carlo numerical simulations in the following scenarios are conducted:

1) Various SNRs - we made use of four levels of SNR (-5, 0, 5 and 10 dB) with only one patch source around $6\,\mathrm{cm}^2$ to evaluate the robustness of our proposed ESI method to noise levels;
2) Various number of channels - we considered using data with varying numbers of channels with SNR = 5 dB, including 100% (62 channels), 75% (47 channels), 50% (31 channels), and 25% (16 channels) to evaluate the robustness of our proposed ESI method to different amounts of data. For each simulation, channels of all non-complete cases were randomly selected.

For each case, we conducted 50 Monte Carlo simulations.

3.2 Performance Metrics

To fully evaluate the performance of ESI algorithms, we carry our four performance metrics. (1) The area under the receiver operating characteristic (ROC) curve (AUC) [4,11], describing the sensitivity and specificity of the reconstructed sources. (2) Spatial dispersion (SD) [11,12], measuring the spatial blurring of the reconstructed sources w.r.t. the ground truth. (3) The distance of localization error (DLE) [9,12], measuring the localization error of the reconstructed sources w.r.t. the ground truth. (4) The normalized relative mean square error (nRMSE) [10], measuring the relative squared error between the normalized reconstructed sources and the normalized ground truth.

Details of four performance metrics can be found in [12]. In general, higher AUC values with lower SD, DLE and nRMSE values imply better performance of the ESI methods. The significance is assessed using the Kruskal-Wallis test. Suppose that the statistic from the Kruskal-Wallis test is significant, we will further conduct Wilcoxon rank sum tests to determine whether VSSI-L_p yields significantly superior estimations against each benchmark algorithm. The Otsu's threshold is employed to visualize the imaging results [10,12].

4 Results

4.1 Simulation Results Analysis

Effect of Different p-values. For the L_p-norm-based methods, the value of p primarily affects the sparsity of the solutions. Here, we compared the performance of VSSI-L_p with various p-values from 0.1 to 0.9 with one patch source under the SNR = 5 dB, to test the influence of the p-value. Figure 1 depicts the performance metrics under different values of p. For $p < 0.5$, the L_p-norm enforced the sparsity too aggressively, leading to a high error rate in source estimation, evidenced by the low AUC, and large DLE, SD, and nRMSE values.

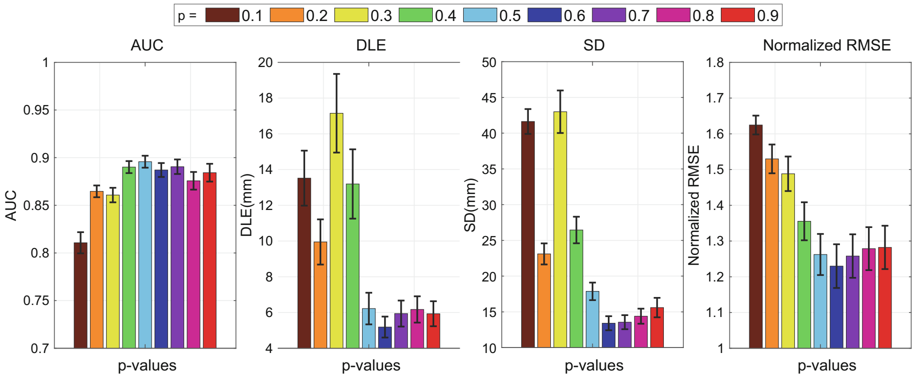

Fig. 1. Performance metrics under various values of p. The figure shows the Mean ± SEM (standard error of the mean) of the results for 50 Monte-Carlo simulations.

Conversely, the performance of VSSI-L_p remains stable when $p \geq 0.6$. Consequently, for VSSI-L_p, the p-value in the later simulations are empirically selected as 0.6.

Effect of SNRs. Figure 2 presents the performance metrics under various SNRs. As the SNR increases, all algorithms show improved performance, indicated by the increased AUC ($p < 0.05$), decreased DLE ($p < 0.05$), SD ($p < 0.05$) and nRMSE ($p < 0.05$) values. Because L_1 and L_p-norm-based methods enforce sparsity on the original domain, they always produce point estimations, resulting in the lowest SD values at all SNR levels. However, the L_1 and L_p-norm regularizations produce many false estimations, indicated by the large DLE values, and provide little information about source extents, indicated by the lowest AUC values. VSSI-L_p outperforms VB-SCCD, wMNE and LORETA, indicated by the largest AUC, lowest SD and nRMSE values.

Figure 3 provides an imaging example under different SNRs. As expected, wMNE and LORETA produce too diffused estimations, while the L_1-norm and L_p constraint in the original source domain obtained several point sources around

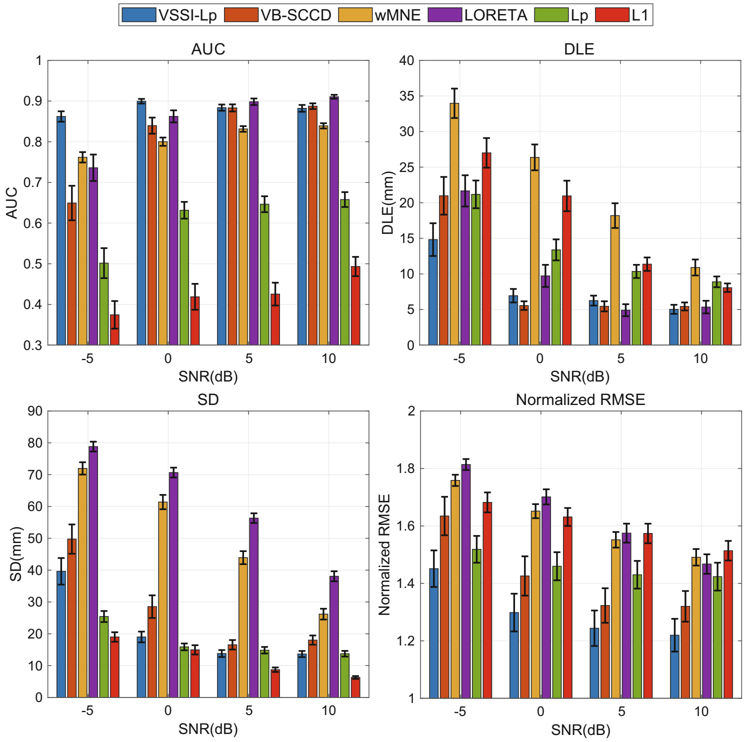

Fig. 2. Performance metrics of various SNRs. This figure shows the Mean ± SEM of the results for 50 Monte-Carlo simulations.

or in the ground truth. VB-SCCD shows better estimations than the other benchmark methods, although it provides some spurious sources around the actual activities. Among all the ESI methods, the reconstructions by the proposed VSSI-L_p are the most accurate in matching the ground truth.

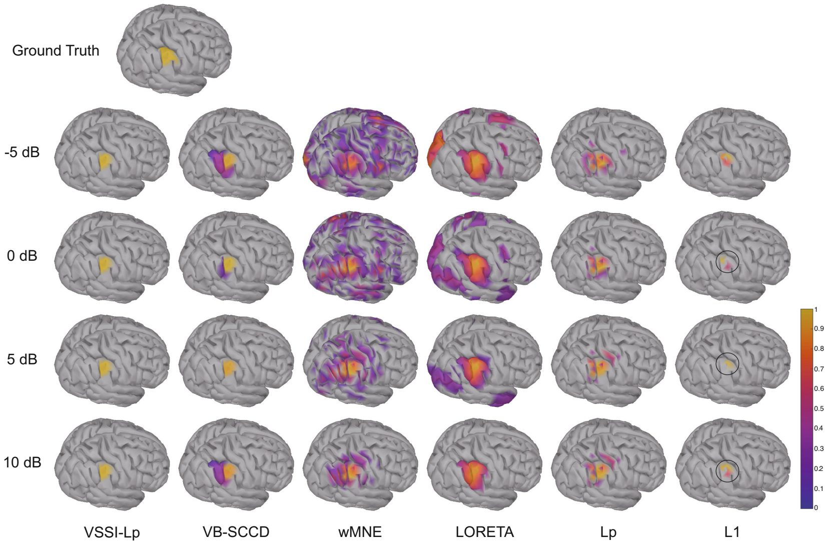

Fig. 3. Imaging example under different SNR levels. The thresholds of the estimated maps are obtained using Ostu's method.

Effect of the Number of Channels. Figure 4 presents the performance metrics under different numbers of EEG channels. As the number of channels decreases, the performance of all methods declines due to the loss of measurement information. VSSI-L_p exhibits good robustness and provides more accurate information on extended sources than other methods even with some missing data, indicated by larger AUC ($p < 0.05$) and lower DLE ($p < 0.05$), SD ($p < 0.05$, except for L_1-norm) and nRMSE ($p < 0.05$) values.

4.2 Real Data Result Analysis

In this subsection, we utilized the public EEG dataset to further assess the practical efficacy of VSSI-L_p, which is the epilepsy EEG data from Brainstorm. Detailed descriptions can be found at https://neuroimage.usc.edu/brainstorm/DatasetEpilepsy. In this work, we followed the tutorial of Brainstorm to derive the head model, lead-field matrix and EEG data for source localization. The EEG data is presented in Fig. 5(a), which is an average of 58 tails, and the data at the peak (0 ms) is used for source imaging. Figure 5(b) presents the

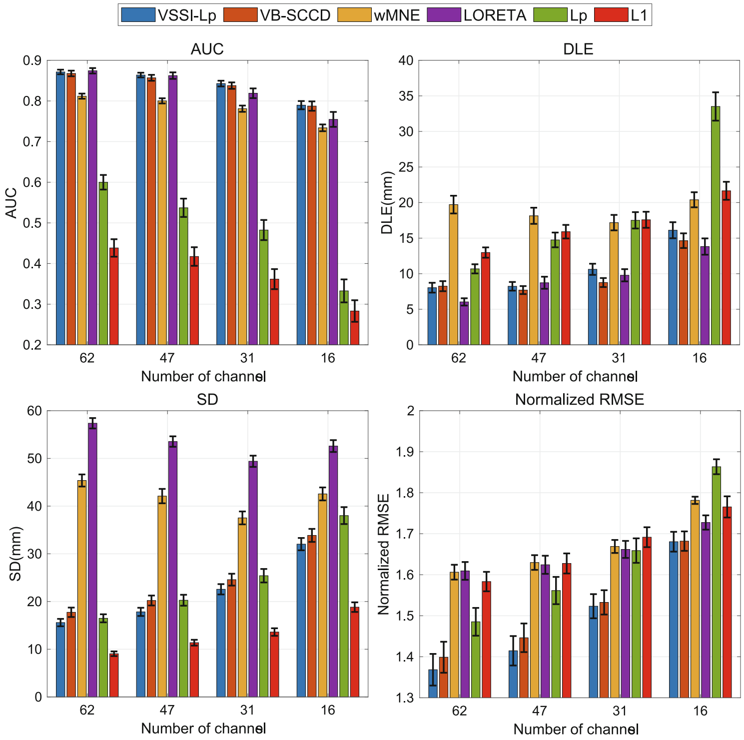

Fig. 4. Performance metrics of various number of channels. This figure shows the Mean ± SEM of the results for 50 Monte Carlo simulations.

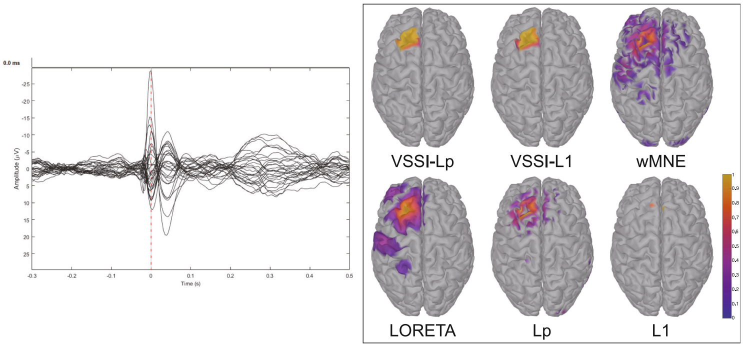

(a) Averaged EEG data

(b) ESI result at 0 ms

Fig. 5. Estimated sources of epilepsy data. (a) is the waveforms of averaged EEG data; (b) is the result of each algorithm at 0 ms.

imaging results. wMNE and LORETA provide diffused estimations, while the result of LORETA is smoother. L_1-norm regularization obtains 2 point sources, and L_p-norm regularization yields several incoherent point sources around the left frontal lobe. Results of VSSI-L_p and VB-SCCD provide clear information about the location and extent of potential sources, which conform to clinical findings in [5].

5 Discussion and Conclusion

Here in this work, we proposed a new ESI method, VSSI-L_p, to reconstruct the location and extent of brain activity. VSSI-L_p method enforces the sparsity of potential brain sources using the L_p-norm regularization in the variation domain. By utilizing the ADMM and GST algorithms, the solution of VSSI-L_p can be efficiently obtained. Numerical simulations and real data analysis reveal the superior performance of VSSI-L_p.

Due to the highly under-determined nature of ESI, such methods are difficult to work out. Even worse, it is essential for neuroscience and neurology applications to infer the spatial distribution of potential brain sources from limited measurements. Methods based on L_2-norm constraint, such as wMNE and LORETA, produce too blurred and diffused results, indicated by the large DLE and SD values in Fig. 2. Methods based on L_1-norm and L_p-norm improve the spatial resolution of their estimations by enforcing sparsity in the original source domain. However, these conventional sparse constrained methods provide little information on the extent of brain activity because they miss the most active sources on the cortex.

To estimate the localization and extent of potential extended sources, VB-SCCD [4] employed L_1-norm sparse constraint in the spatial variation domain which significantly improved the reconstructions of extended sources. However, as suggested in [2], VB-SCCD over-estimates the extent of cortical activities, especially for sources with small extents. This may be because the mathematical properties of L_1-norm make it not sparse enough [3]. To enforce sparsity more aggressively, we proposed VSSI-L_p, which employed the L_p-norm ($0 < p < 1$) instead of the L_1-norm regularization in the variation domain. Results of Monte Carlo simulations demonstrate the superiority of VSSI-L_p over VB-SCCD with higher AUC values and lower DLE, SD, and nRMSE values in most cases.

In this work, the regularization parameter, λ, was selected using cross-validation. In our future work, we plan to investigate using the Bayesian probability framework to model VSSI-L_p and allow the model to infer the parameters automatically. Additionally, we will also apply the proposed method for brain disease diagnosis, cortical network analysis and fine motor imagery decoding.

Acknowledgments. This work was supported in part by the National Natural Science Foundation of China under Grants 62136002, and the Natural Science Foundation of Chongqing under Grant CSTB2022NSCQ-MSX0291 and cstc2022ycjh-bgzxm0004.

References

1. Bai, X., Towle, V.L., He, E.J., He, B.: Evaluation of cortical current density imaging methods using intracranial electrocorticograms and functional MRI. Neuroimage **35**(2), 598–608 (2007)
2. Becker, H., Albera, L., Comon, P., Gribonval, R., Wendling, F., Merlet, I.: Brain-source imaging: from sparse to tensor models. IEEE Signal Process. Mag. **32**(6), 100–112 (2015)
3. Chartrand, R., Staneva, V.: Restricted isometry properties and nonconvex compressive sensing. Inverse Prob. **24**(3), 035020 (2008)
4. Ding, L.: Reconstructing cortical current density by exploring sparseness in the transform domain. Phys. Med. Biol. **54**(9), 2683 (2009)
5. Dümpelmann, M., Ball, T., Schulze-Bonhage, A.: sLORETA allows reliable distributed source reconstruction based on subdural strip and grid recordings. Hum. Brain Mapp. **33**(5), 1172–1188 (2012)
6. Fang, T., et al.: Decoding motor imagery tasks using ESI and hybrid feature CNN. J. Neural Eng. **19**(1), 016022 (2022)
7. He, B., Sohrabpour, A., Brown, E., Liu, Z.: Electrophysiological source imaging: a noninvasive window to brain dynamics. Annu. Rev. Biomed. Eng. **20**, 171–196 (2018)
8. Hou, Y., Zhou, L., Jia, S., Lun, X.: A novel approach of decoding EEG four-class motor imagery tasks via scout ESI and CNN. J. Neural Eng. **17**(1), 016048 (2020)
9. Liu, K., Wang, Z., Yu, Z., Xiao, B., Yu, H., Wu, W.: WRA-MTSI: a robust extended source imaging algorithm based on multi-trial EEG. IEEE Trans. Biomed. Eng. **70**(10), 2809–2821 (2023)
10. Liu, K., Yu, Z.L., Wu, W., Gu, Z., Li, Y.: Imaging brain extended sources from EEG/MEG based on variation sparsity using automatic relevance determination. Neurocomputing **389**, 132–145 (2020)
11. Liu, K., Yu, Z.L., Wu, W., Gu, Z., Li, Y., Nagarajan, S.: Bayesian electromagnetic spatio-temporal imaging of extended sources with Markov random field and temporal basis expansion. Neuroimage **139**, 385–404 (2016)
12. Liu, K., Yu, Z.L., Wu, W., Gu, Z., Li, Y., Nagarajan, S.: Variation sparse source imaging based on conditional mean for electromagnetic extended sources. Neurocomputing **313**, 96–110 (2018)
13. Lucka, F., Pursiainen, S., Burger, M., Wolters, C.H.: Hierarchical Bayesian inference for the EEG inverse problem using realistic FE head models: depth localization and source separation for focal primary currents. Neuroimage **61**(4), 1364–1382 (2012)
14. Ou, W., Hämäläinen, M.S., Golland, P.: A distributed spatio-temporal EEG/MEG inverse solver. Neuroimage **44**(3), 932–946 (2009)
15. Pascual-Marqui, R.D., Michel, C.M., Lehmann, D.: Low resolution electromagnetic tomography: a new method for localizing electrical activity in the brain. Int. J. Psychophysiol. **18**(1), 49–65 (1994)
16. Sohrabpour, A., He, B.: Exploring the extent of source imaging: recent advances in noninvasive electromagnetic brain imaging. Curr. Opin. Biomed. Eng. **18**, 100277 (2021)
17. Sohrabpour, A., Lu, Y., Worrell, G., He, B.: Imaging brain source extent from EEG/MEG by means of an iteratively reweighted edge sparsity minimization (IRES) strategy. Neuroimage **142**, 27–42 (2016)

18. Tadel, F., Baillet, S., Mosher, J.C., Pantazis, D., Leahy, R.M.: Brainstorm: a user-friendly application for MEG/EEG analysis. Comput. Intell. Neurosci. **2011**, 1–13 (2011)
19. Tibshirani, R.: Regression shrinkage and selection via the Lasso. J. Roy. Stat. Soc. Ser. B (Methodol.) **58**(1), 267–288 (1996)
20. Wang, Y., Yin, W., Zeng, J.: Global convergence of ADMM in nonconvex nonsmooth optimization. J. Sci. Comput. **78**, 29–63 (2019)
21. Zuo, W., Meng, D., Zhang, L., Feng, X., Zhang, D.: A generalized iterated shrinkage algorithm for non-convex sparse coding. In: Proceedings of the IEEE International Conference on Computer Vision, pp. 217–224 (2013)